FINDING EXTREME HIGH-REDSHIFT GALAXIES USING THE 3D-HST SURVEY

An Undergraduate Research Scholars Thesis

by

JULIA TILLER [1]

Submitted to the LAUNCH: Undergraduate Research office at
Texas A&M University
in partial fulfillment of the requirements for the designation as an

UNDERGRADUATE RESEARCH SCHOLAR

Approved by
Faculty Research Advisor Casey Papovich

May 2021

Major: Physics [1]

RESEARCH COMPLIANCE CERTIFICATION

Research activities involving the use of human subjects, vertebrate animals, and/or biohazards must be reviewed and approved by the appropriate Texas A&M University regulatory research committee (i.e., IRB, IACUC, IBC) before the activity can commence. This requirement applies to activities conducted at Texas A&M and to activities conducted at non-Texas A&M facilities or institutions. In both cases, students are responsible for working with the relevant Texas A&M research compliance program to ensure and document that all Texas A&M compliance obligations are met before the study begins.

I, Julia Tiller [1], certify that all research compliance requirements related to this Undergraduate Research Scholars thesis have been addressed with my Research Faculty Advisor prior to the collection of any data used in this final thesis submission.

This project did not require approval from the Texas A&M University Research Compliance & Biosafety office.

TABLE OF CONTENTS

ABSTRACT

Finding Extreme High-Redshift Galaxies Using the 3D-HST Survey

Julia Tiller [1]
Department of Physics and Astronomy [1]
Texas A&M University

Research Faculty Advisor: Casey Papovich
Department of Physics and Astronomy
Texas A&M University

In the very beginning stages of the universe, stars and galaxies began to form in their neutral intergalactic medium (IGM) of Hydrogen. Because these galaxies are clouded in their IGM, Lyman-α emission lines are absorbed and obscured as a result. But with the 3D Hubble Space Telescope Survey (3D-HST Survey), we can use its large photometric selection of approximately 100,000 galaxies and low resolution grism slit-less spectroscopy to probe these distant galaxies. The survey allows us to take near-infrared spectra of many objects simultaneously, generating the deep data needed to find a selection of high redshift candidates. A novel method is introduced to detect and quantify faint emission lines by using Bayesian techniques. Previous work was done to systematically analyze the 100,000 galaxies, and a preliminary set of 29 promising candidates were presented. In order to remove false positives from this selection, we validated the input photometry through an updated version of EAZY, and compared with the image cutouts of each of these objects, along with the previously obtained grism redshifts. Of the preliminary 29 galaxies, 22 were promising candidates and 7 were removed as false positives. Further analysis and spectroscopic confirmation are needed to fully vet this method for future grism based missions.

DEDICATION

To Maxwell Throm, who sat along side me while I wrote my thesis as he was writing his own.

ACKNOWLEDGMENTS

Contributors

I would like to thank my faculty advisor, Dr. Casey Papovich, and my collaborators, John Weaver and Dr. Gabriel Brammer, for their guidance and mentorship throughout this research under the DAWN-IRES Scholars program through the Cosmic DAWN Center in Copenhagen, Denmark.

Thanks also go to my friends and colleagues and the department faculty and staff for making my time at Texas A&M University a great experience.

Finally, thanks to my family for their encouragement, patience, and love.

This work is based on observations taken by the 3D-HST Treasury Program (GO 12177 and 12328) with the NASA/ESA HST, which is operated by the Association of Universities for Research in Astronomy, Inc., under NASA contract NAS5-26555.

All other work conducted for the thesis was completed by the student independently.

Funding Sources

This work was also made possible in part by the DAWN-IRES Scholars Program, who sponsored my research and travel.

NOMENCLATURE

Lα	Lymann Alpha Emission Line
3D-HST	3D Hubble Space Telescope
SED	Spectral Energy Distribution
WFC3	Wide Field Camera 3
IGM	Intergalactic Medium

1. INTRODUCTION

1.1 Motivation

The universe has gone through two significant phase shifts in its history. The first shift, Recombination, was within the first 400,000 years of the universe, where charged electrons and protons first became bounded to neutral hydrogen. The universe then went through the dark ages where space was opaque.

The reionization epoch occurred between 150 million and one billion years after the big bang. After the dark ages, the universe began to cool and gravity pulled clumps of neutral hydrogen together into clouds. This is when the first stars and galaxies began to form and would re-ionize the hydrogen around it, hence the name reionization. Our goal is to ultimately improve our understanding of the epoch of reionization by finding these early-universe galaxies.

The photons from the Lyman light energy transitions radiating from these early stars and galaxies are absorbed and obscured by neutral intergalactic medium (IGM). We are looking for galaxies that have "bubbles" of ionized Hydrogen that allows for $L\alpha$ transmission, but it is incredibly rare to find these galaxies such that they have a favorable IGM that allows the Lyman-alpha emission's faint light to be captured through the grism in the Hubble Space Telescope.

1.2 Data

The data we will use to probe these distant galaxies is the 3D Hubble Space Telescope Survey (3D-HST Survey) [1] [2]. This survey has a few important characteristics that will give us the best opportunity at finding these extreme high-redshift galaxies, one being it contains a very large sample size of approximately 100,000 galaxies.

In addition, it covers a wide range of the sky, about 70% of the famous CANDELS fields [3] [4]. CANDELS is a deep broad-band imaging survey that covers five famous fields, AEGIS, UDS, COSMOS, GOODS-N, and GOODS-S.

In combination with a large sample size of galaxies, a large area of sky covering, the 3D-HST

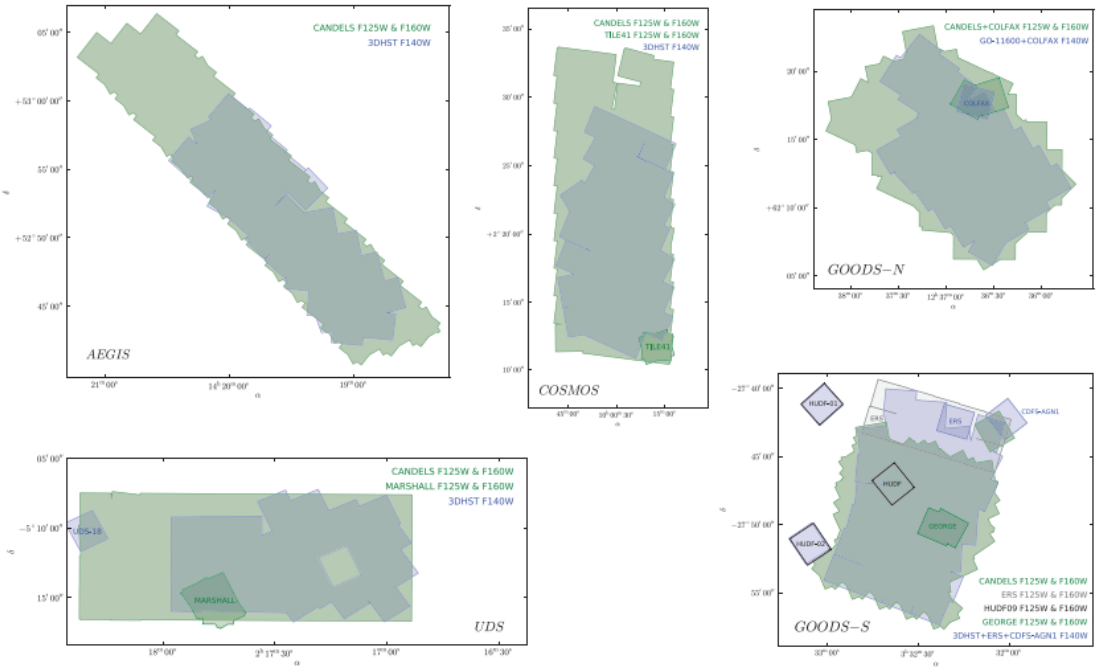

Figure 1.1: CANDELS mosaics displaying layouts of the WFC3 observations [3].

survey also uses Low-Resolution Grism Spectroscopy, which allows us to looks at many, many objects or galaxies all at once. This results in rich and deep data, but the quality of the image is not a precise, hence why it is "low-resolution", shown in Figure 1.2. We much prefer low resolution images since we use complex statistical analysis with the data and numbers.

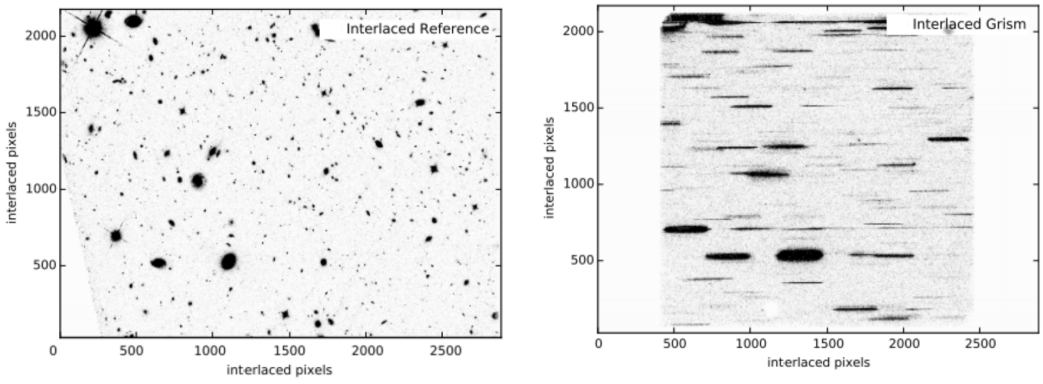

Figure 1.2: COSMOS-04 pointing. The left image is the interlaced direct reference image from CANDELS+3DHST mosaic. The right image is the observed interlaced grism [2].

1.3 Processes

In section II, Methods, we introduce and elaborate on a novel emission-line fitting program, in which we boost statistically insignificant emission lines to become statistically significant through Bayesian analysis methods [5]. This method shows promise because from the sample of approximately 100,000 galaxies, it was narrowed down to only 29 potential high-redshift candidates.

In order to remove false positives from this selection of 29 galaxies, we validated the input photometry through an updated version of EAZY, a photometric redshift-fitting program, and compared the image cutouts of each of these objects along with the previously obtained grism redshifts [6]. Of the preliminary 29 galaxies, 17 were promising candidates, 9 were unsure, and 3 were removed. The 9 that were unsure underwent further analysis to see if there was a chance at improving their data and models in order to give some promise. From the 9, 4 were categorized as false positives. Thus, we obtained a total of 22 promising high redshift galaxies. Further analysis and spectroscopic confirmation are needed to fully vet this method for future grism based missions.

2. METHODS

2.1 Novel Emission Line Fitting Method

The purpose of the novel emission line search technique was to create large spectroscopic data sets for slitless spectroscopy [5]. The Bayesian nature of the program allowed for more probabilistic emission line identifications, such as redshift estimates based on photometric priors. It is usually difficult to obtain clean and useful information from slitless grism spectroscopic data. Contamination from other unrelated objects in space, especially in densely populated areas, makes detailed findings very challenging.

Emission lines from galaxies are the easiest and most interesting features that we can detect from faint objects. This line detection works by, based on the input photometry, obtaining a redshift probability that is convolved along the grism and compared with a set of expected emission lines. This effectively boosts statistically insignificant, or faint, emission lines and pinpoints a high redshift, the grism redshift. In previous work done by John Weaver, he was able to use this novel method with the 3D-HST Survey data. The line detection program systematically analyzed the 100,000 galaxies from the survey and 2,000 of them were potential candidates.

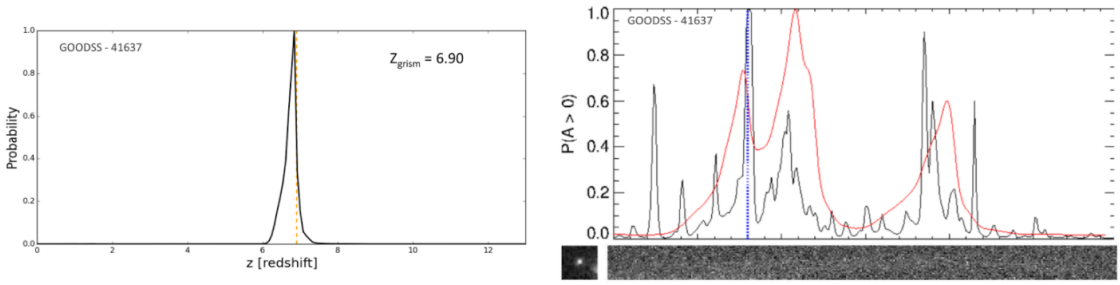

Figure 2.1: (Left) Redshift probability distribution for object 41637 from the GOODS-S field. (Right) Object's probability distribution convolved with a set of expected high redshift emission lines (red) with a grism detection (blue). The image cutout along with its 2D grism image is below.

Since this method is very new and unique, Maseda concluded in his research that there were some grism exposures that mimicked emission features, due to potential un-modeled or under-predicted spectral contamination. Weaver went through, by hand, the 2,000 remaining galaxies and looked at the spectral features and found only 29 potential high redshift candidates.

The line detection program is inherently designed to detect a high-redshift grism detection within the redshift probability prior because that is all the data the program is fed to begin with. It is incredibly important that the photometry needs to be correct and validated otherwise, the detected grism redshifts will be flawed.

2.2 Validating Input Photometry

Since Weaver's previous research, there have been many updated tools to validate the photometry from the 3D-HST dataset. This is the data that needs to be correct or it can cause skewed results for finding potentially high redshift galaxies. We begin by running the data through EAZY, a photometric redshift fitting program designed to be accurate without having complete spectroscopic data [6].

Within this program the models used to fit the data are the Flexible Stellar Population Synthesis (FSPS) models [7]. These have since been updated and have gained more models as well. Ultimately, the output most important pertaining to our research are the SED's generated for a particular object. SED's are a Flux ($f_\lambda = 10^{-19}\ erg/s/cm^2$), verses the observed wavelength ($\lambda_{obs} = microns$) figure. From this SED, as seen in Figure 2.2, we can see the photometric points from the data along the modeled emission lines. A continuum break at a specific wavelength is often noticed and the redshift can be derived for a specific object. Once again, we depend on the photometric points to constrain this break in the figure and to follow along the model.

2.3 Redshift Probability Distributions

In addition to generating the SED's, we obtain the redshift probability distributions for each object. Based on different prior models, we can generate a probability distribution for the redshift. This is important in order to evaluate the previous work done by Weaver to ensure that the results are comparable.

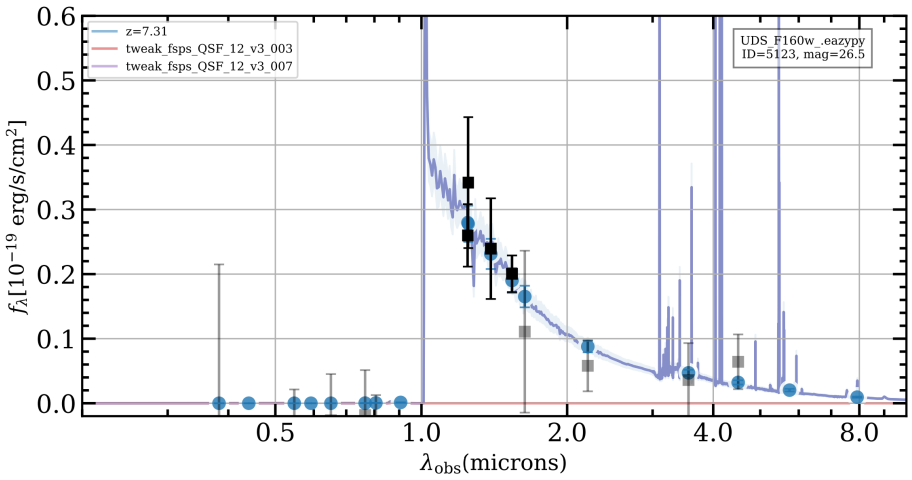

Figure 2.2: Spectral Energy Distribution (SED) for object 5123 from the UDS field.

There are two different sets of prior models to feed into EAZY, a F160W prior, and a Flat prior. The F160W prior comes from the HST Survey and this inherently gives an assumption about the likelihood of each redshift based on past "experience".

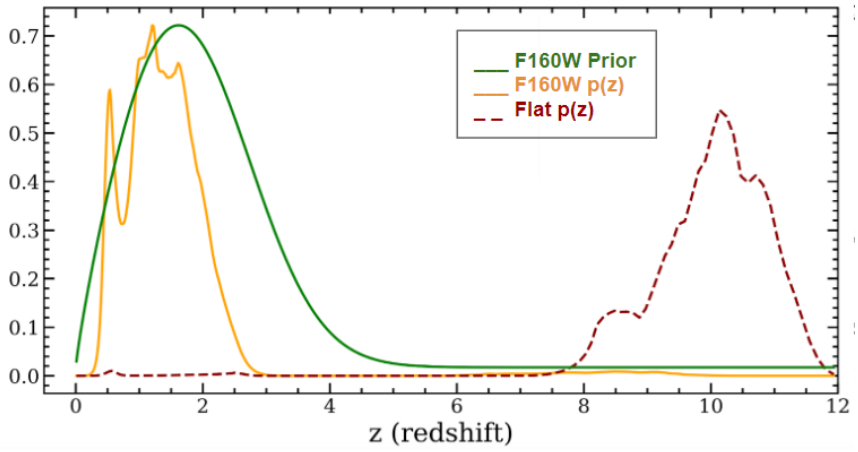

Figure 2.3: F160W prior and redshift probability distributions for object 17931 from the AEGIS field.

From Figure 2.3, we can see that the probability distribution $(p(z))$, from a F160W prior is right skewed, which makes intuitive sense since the liklihood that the object is going to be a high

redshift candidate is reasonably low, being that they are extremely rare.

On the other hand, a flat prior assumes that any redshift is equally likely and the data will drive the results more. This can be interpreted as the models being "less informed" thus we can assume that using a flat prior might result in potentially assuming the galaxy to be at a higher redshift.

2.4 Image Cutouts

The actual images of these galaxies from the 3D-HST Survey are also needed in order to further vet this method. Although these galactic sources are faint, there should be a visible dot deep within the fields we are looking at. This is further proof that a galaxy potentially exsits, and not just noise or space.

Each photometric point corresponds to a point on our generated SED's. Certain Hubble Space Telescope filters are specialized to see either more local or faint objects.

When we look at $L\alpha$ galaxies, the emissions will be absorbed until the "lyman break" at 1216 Å, as seen in Figure 2.4. Visually this is seen as the "dropout method" since once we look beyond

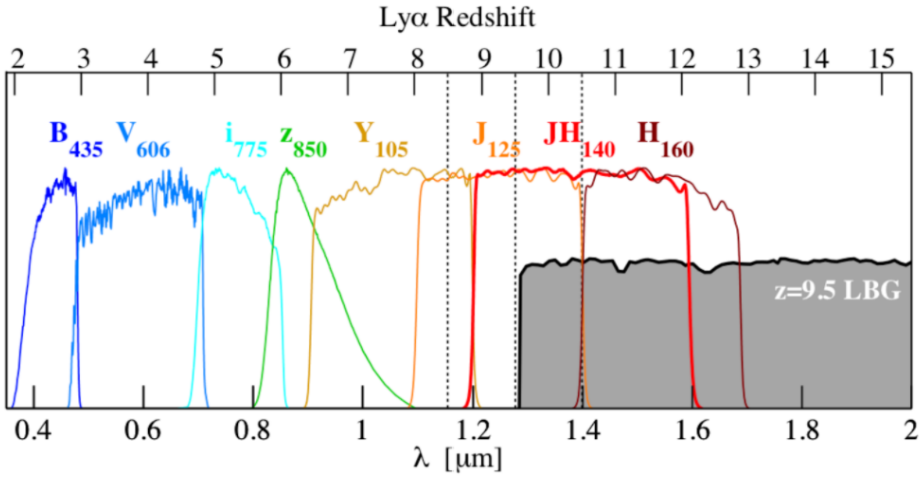

Figure 2.4: In the gray area of the figure, there is a lyman break galaxy at redshift 9.5. Its emissions are stronger and brighter at wavelengths longer than the lyman break [8].

the break, the emission becomes brighter and more easily detectable, shown in Figure 2.5. It can be used to help determine if the galaxy is high redshift or not [8].

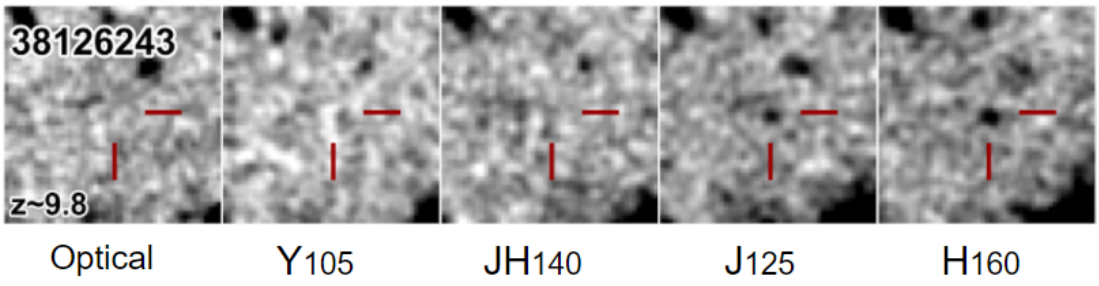

Figure 2.5: An object at redshift of 9.8 can be captured in the J and H bands [8].

The filters we then focus on in order to find the higher redshift galaxies are going to fall within the J and JH bands. In addition, we will also be looking for other high redshift emission lines that are not Hydrogen, and won't be absorbed in this epoch. These are some of the more exotic emission lines to find interesting high redshift objects.

3. ANALYSIS & RESULTS

3.1 Initial Results

After validating the photometry using updated versions of EAZY and FSPS models, Table 3.1 displays the data for the photometric redshifts we have obtained for the 29 potential high redshift candidates.

Table 3.1: Initial Results

	Grism Redshift	**EAZY Redshift**
Range	0.00 - 8.75	1.31 - 11.49
Median	6.23	5.01

Since the range for the photometric redshifts in these objects is so large, we really need to ensure that there is not any data skewing these results, whether that means looking at the photometric points or improving the models.

Of the 29 potential high redshift galaxies, 3 were immediately removed and categorized as false positives due to extreme noise in their images, displayed in Figure 3.1. Some have a clear diffraction spike from a nearby object, likely a star. This skews the data to be completely unreliable, which makes it easy to categorize these as false positives, shown in Figure 3.1.

Some objects, on the other hand, are less easily classified even with all of the data we have gathered. 9 of these galaxies need to be inspected further, which we will discuss in the next section.

From the initial run through, we have successfully gathered 17 promising high redshift galaxies.

3.2 Iterative Goodness of Fit Testing

There are numerous variables to consider with these remaining galaxies. Some of them have a well fitting SED model, but few photometric points, and some might have an unconvincing model,

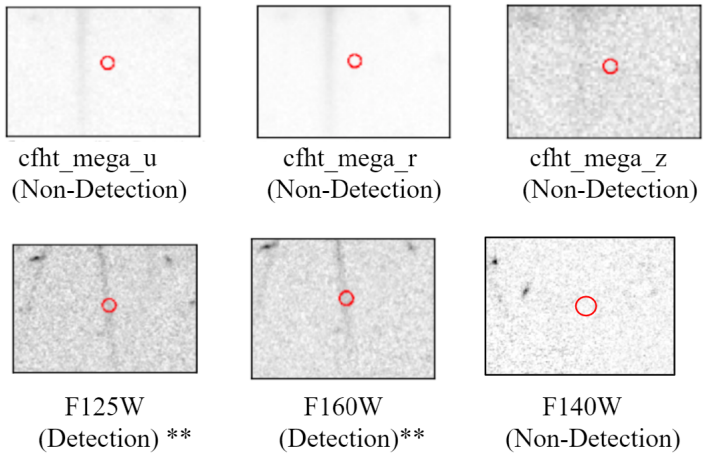

Figure 3.1: For Object 17931 from the AEGIS field, we see a clear diffraction spike which impairs the data.

Table 3.2: 17 Promising Candidates

Object ID	**Field**	**EAZY Redshift (flat prior)**	**Grism Redshift**
20187	AEGIS	8.03	7.30
34307	AEGIS	7.23	6.97
5956	COSMOS	4.80	5.29
7696	COSMOS	6.13	6.24
9338	COSMOS	4.62	4.51
10912	COSMOS	5.37	5.54
13141	COSMOS	5.04	4.77
13254	COSMOS	4.62	4.62
25077	COSMOS	5.69	5.75
24946	GOODSS	5.71	6.25
41637	GOODSS	6.67	6.90
23245	GOODSN	5.51	5.58
29638	GOODSN	6.36	6.23
5123	UDS	7.81	8.08
33192	UDS	8.55	6.81
34012	UDS	5.04	4.78
39355	UDS	6.30	6.27

but clear photometric detections. If we can carve out more information from this data set in order to improve the SED models, then these objects can show promise.

To do this, we will calculate the chi-squared (χ^2) distribution for each object, and then iteratively remove one of the filter bands in order to see the weight or impact they have on the model. We calculate the χ^2 distribution for each iteration and plot them on top of each other to see how it impacts the redshift.

$$\chi^2 = \frac{(f_{obs} - Ef_{obs})^2}{(Ef_{obs})^2} \qquad \text{(Eq. 1)}$$

Where f_{obs} is the observed value, and Ef_{obs} is the expected value for the observed value.

This method allows us to quantiativley measure how well our model compares with the photometric data. The redshift is determined by the minima of the χ^2 distribution, which is marked by a vertical line shown in Figure 3.2. It can be seen that there are a couple vertical lines drawn. Although it is less probable, there is exists a different, and more importantly higher, potential redshift for this object.

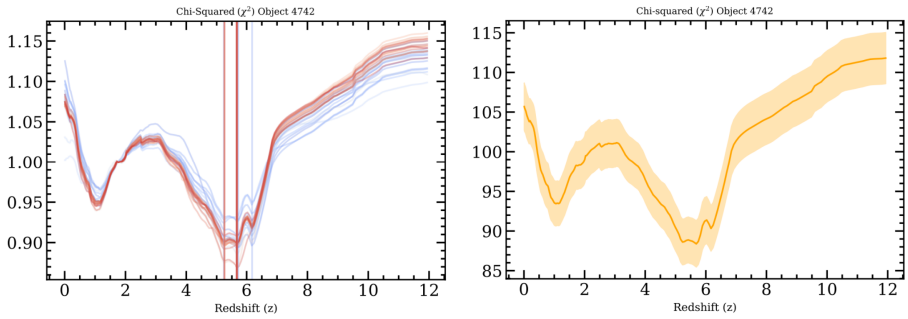

Figure 3.2: (Left) χ^2 Distribution for iterative testing for Object 4742 from the AEGIS field. (Right) The average χ^2 with the standard deviation for object 4742.

We can now re-fit the SED to this higher redshift and see if overall this object looks more promising. Figure 3.3 shows the original SED below the newly fitted model. The continuum break is better constrained with the new fit, and aligns with the emissions in the IRAC filter bands better as well. Since this new potential red-shift showed some improvement, this gives more promise to

this galaxy truly being a high redshift object.

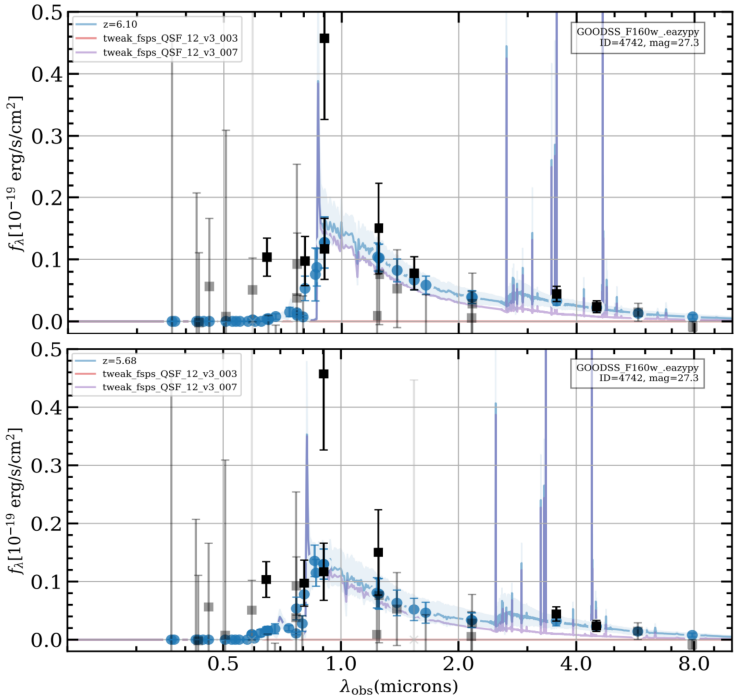

Figure 3.3: (Above) Newly fitted 4742 Object. (Below) Original SED for Object 4742 from the GOODSS field.

This method is repeated for each of the 9 objects, from which 4 were removed as false positives. The remaining 5 are displayed in the Table 3.3. Each χ^2 plot along with an improved SED, if applicable, are displayed in Appendix B.

Table 3.3: 5 New Promising Candidates

Object ID	**Field**	**EAZY Redshift (flat prior)**	**Grism Redshift**
10381	AEGIS	8.02	6.93
4742	GOODSS	5.73	6.53
30607	GOODSS	11.49	6.18
26338	UDS	5.80	5.61
27018	UDS	6.92	8.75

4. CONCLUSION

Overall, we have successfully removed 7 false positives from the original 29 potential high redshift candidate selection, shown in Table 4.1. The SED's, image cutouts, and redshift probabilities for each of the 29 objects are shown in Appendix A.

With 22 promising high redshift galaxies of the 29, we have about 76% accuracy, which is very impressive considering we began from 100,000 galaxies. These results show much promise for the novel line fitting method to be used in other future grism based missions, such as Euclid and the James Webb Space Telescope.

In order to fully vet this process, we seek to obtain spectroscopic confirmation on these galaxies and cross check our results with other reputable catalogs.

Table 4.1: 7 False Positives

Object ID	**Field**	**EAZY Redshift (flat prior)**	**Grism Redshift**
13718	AEGIS	1.88	6.15
17931	AEGIS	10.16	8.17
31282	AEGIS	2.60	7.05
26864	GOODSS	6.23	6.14
27478	GOODSS	9.30	6.05
18763	UDS	2.73	6.83
29028	UDS	10.08	0.00

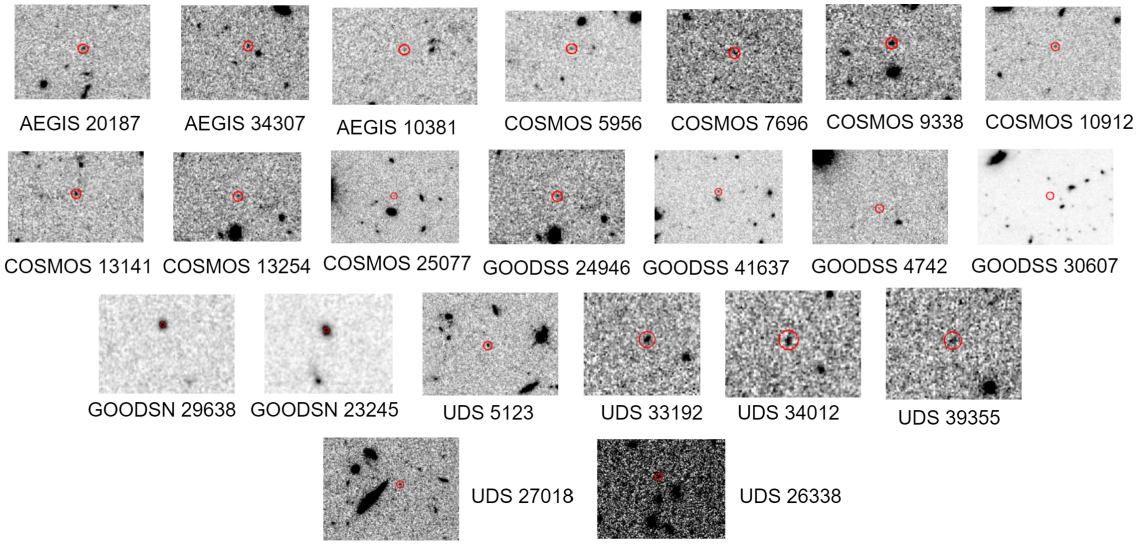

Figure 4.1: 22 promising high redshift galaxies image cutouts.

REFERENCES

[1] G. B. Brammer, P. G. van Dokkum, M. Franx, M. Fumagalli, S. Patel, H.-W. Rix, R. E. Skelton, M. Kriek, E. Nelson, K. B. Schmidt, and et al., "3d-hst: A wide-field grism spectroscopic survey with the hubble space telescope," *The Astrophysical Journal Supplement Series*, vol. 200, p. 13, May 2012.

[2] I. G. Momcheva, G. B. Brammer, P. G. van Dokkum, R. E. Skelton, K. E. Whitaker, E. J. Nelson, M. Fumagalli, M. V. Maseda, J. Leja, M. Franx, and et al., "The 3d-hst survey: Hubble space telescope wfc3/g141 grism spectra, redshifts, and emission line measurements for 100,000 galaxies," *The Astrophysical Journal Supplement Series*, vol. 225, p. 27, Aug 2016.

[3] R. E. Skelton, K. E. Whitaker, I. G. Momcheva, G. B. Brammer, P. G. van Dokkum, I. Labbé, M. Franx, A. van der Wel, R. Bezanson, E. Da Cunha, and et al., "3d-hst wfc3-selected photometric catalogs in the five candels/3d-hst fields: Photometry, photometric redshifts, and stellar masses," *The Astrophysical Journal Supplement Series*, vol. 214, p. 24, Oct 2014.

[4] N. A. Grogin, D. D. Kocevski, S. M. Faber, H. C. Ferguson, A. M. Koekemoer, A. G. Riess, V. Acquaviva, D. M. Alexander, O. Almaini, M. L. N. Ashby, and et al., "Candels: The cosmic assembly near-infrared deep extragalactic legacy survey," *The Astrophysical Journal Supplement Series*, vol. 197, p. 35, Dec 2011.

[5] M. V. Maseda, A. van der Wel, H.-W. Rix, I. Momcheva, G. B. Brammer, M. Franx, B. F. Lundgren, R. E. Skelton, and K. E. Whitaker, "The number density evolution of extreme emission line galaxies in 3d-hst: Results from a novel automated line search technique for slitless spectroscopy," *The Astrophysical Journal*, vol. 854, p. 29, Feb 2018.

[6] G. B. Brammer, P. G. van Dokkum, and P. Coppi, "Eazy: A fast, public photometric redshift code," *The Astrophysical Journal*, vol. 686, p. 1503–1513, Oct 2008.

[7] C. Conroy and J. E. Gunn, "FSPS: Flexible Stellar Population Synthesis," Oct. 2010.

[8] P. A. Oesch, R. J. Bouwens, G. D. Illingworth, I. Labbé, M. Franx, P. G. van Dokkum, M. Trenti, M. Stiavelli, V. Gonzalez, and D. Magee, "Probing the dawn of galaxies atz 9-12: New constraints from hudf12/xdf and candels data," *The Astrophysical Journal*, vol. 773, p. 75, Jul 2013.

APPENDIX A: Object Individual Data

4.1 AEGIS Data

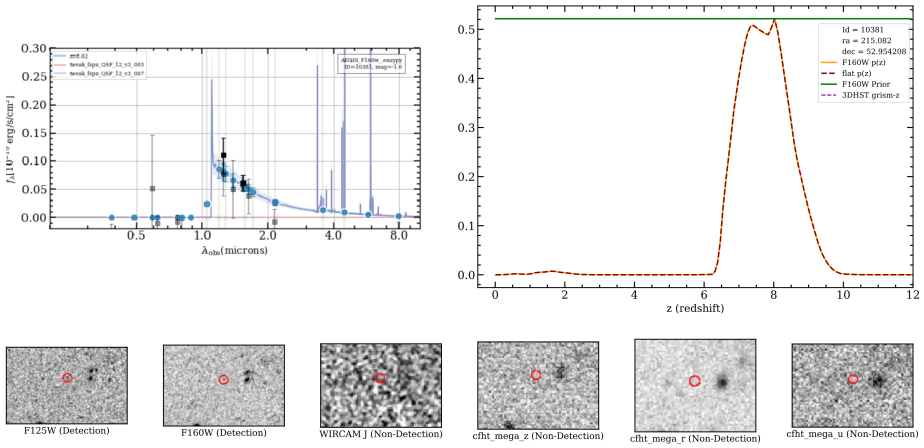

Figure 4.2: Object 10381 from AEGIS, z = 8.02.

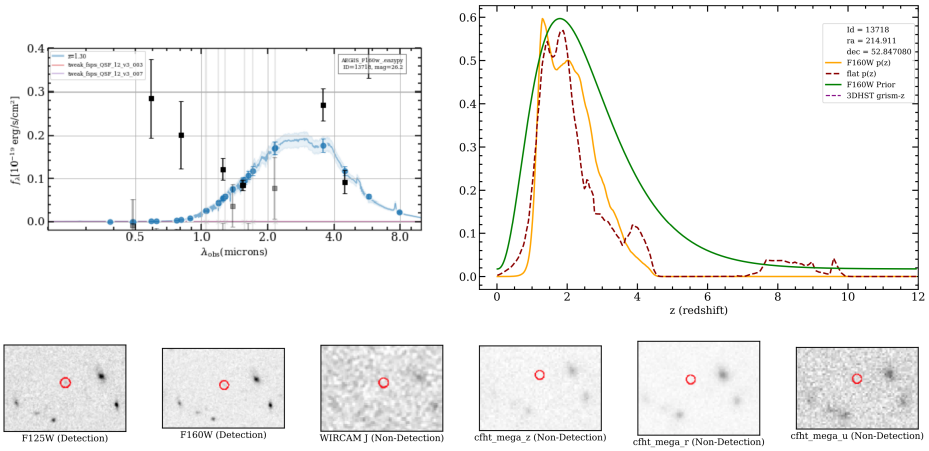

Figure 4.3: Object 13718 from AEGIS, z = 1.30. False Positive

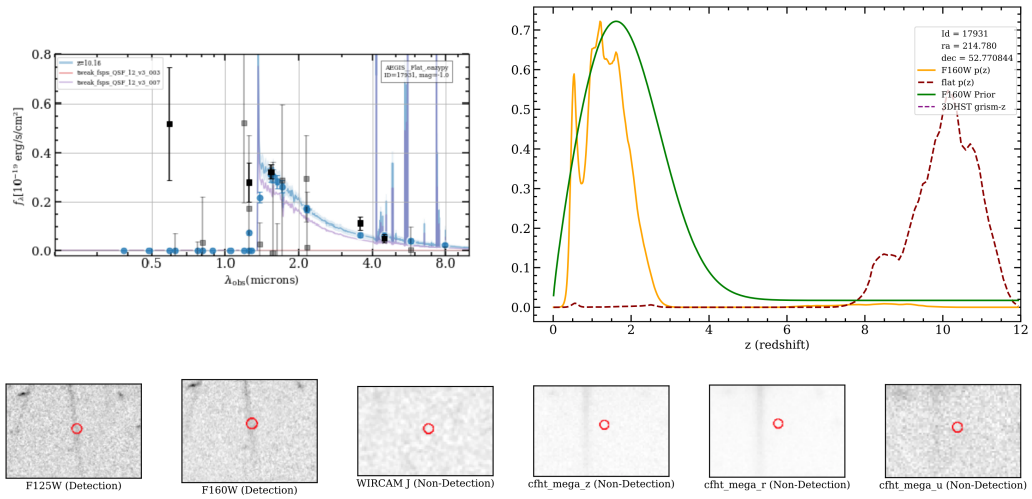

Figure 4.4: Object 17931 from AEGIS, z = 10.16. False positive.

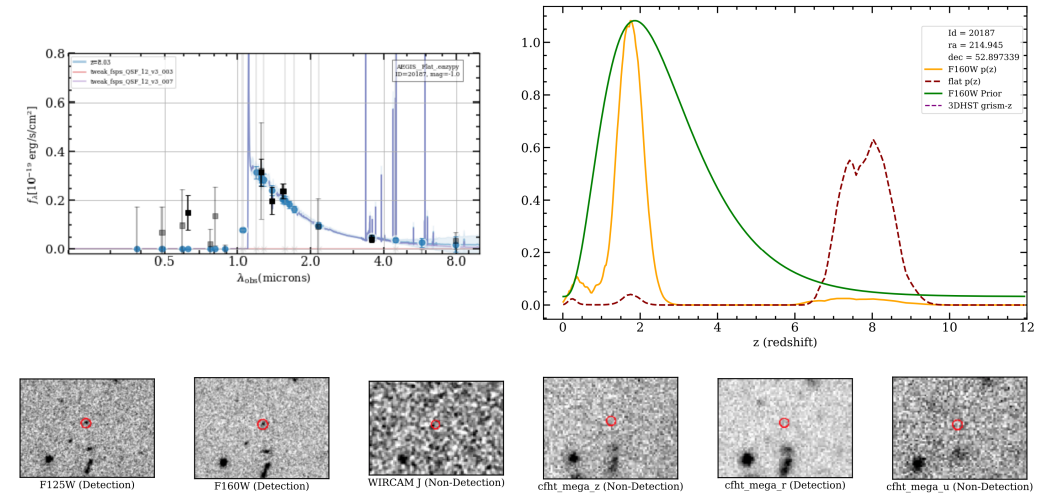

Figure 4.5: Object 20187 from AEGIS, z = 8.03.

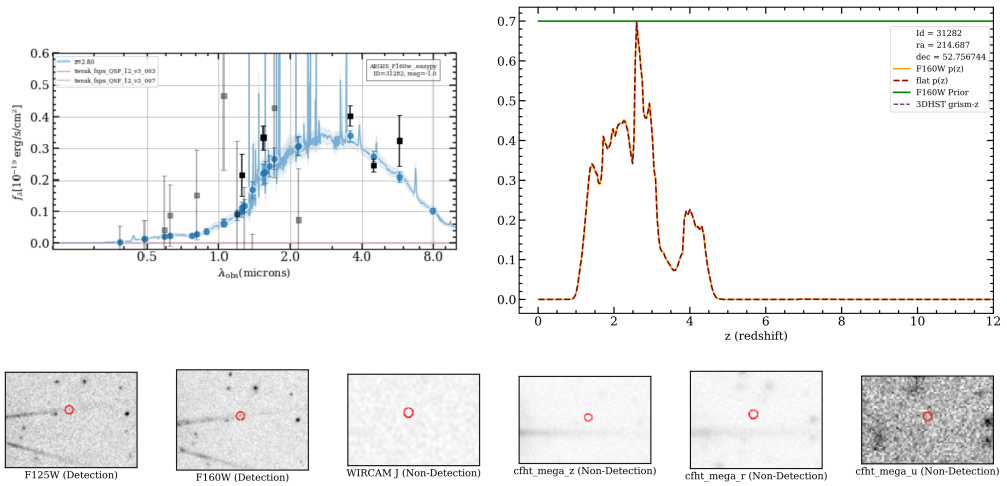

Figure 4.6: Object 31282 from AEGIS, z = 2.60. False positive.

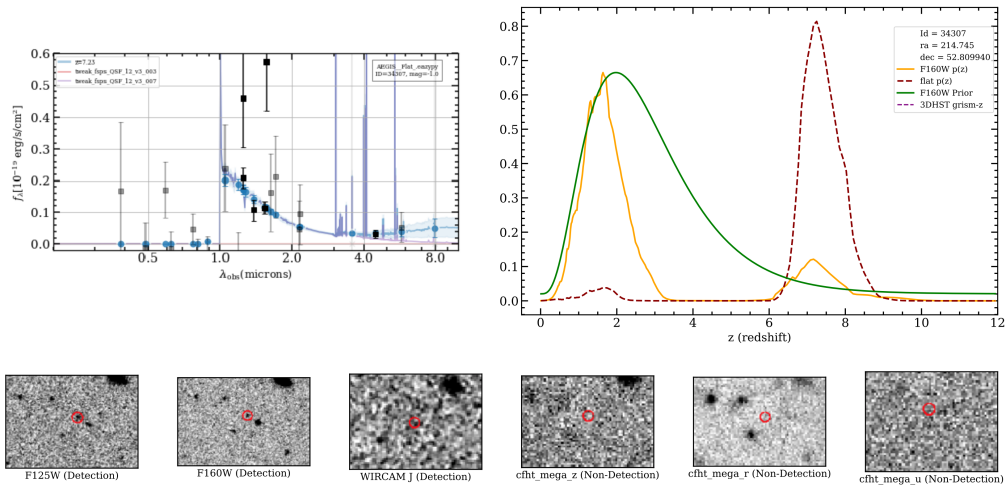

Figure 4.7: Object 34307 from AEGIS, z = 7.23.

4.2 COSMOS Data

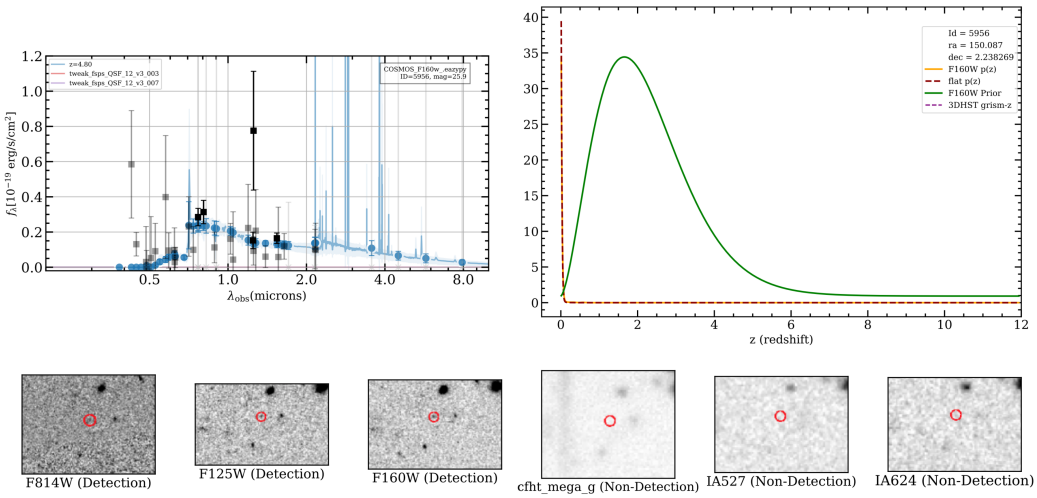

Figure 4.8: Object 5956 from COSMOS, z = 4.80.

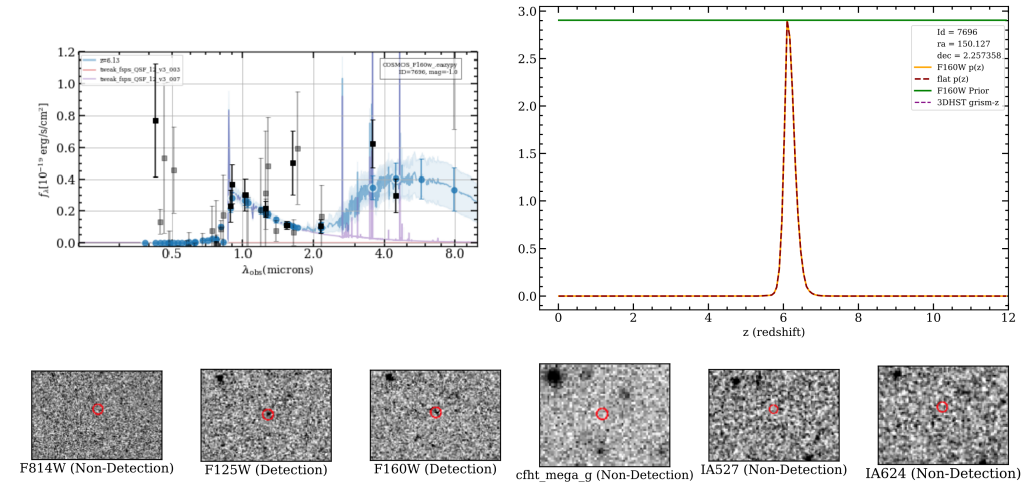

Figure 4.9: Object 7696 from COSMOS, z = 6.13.

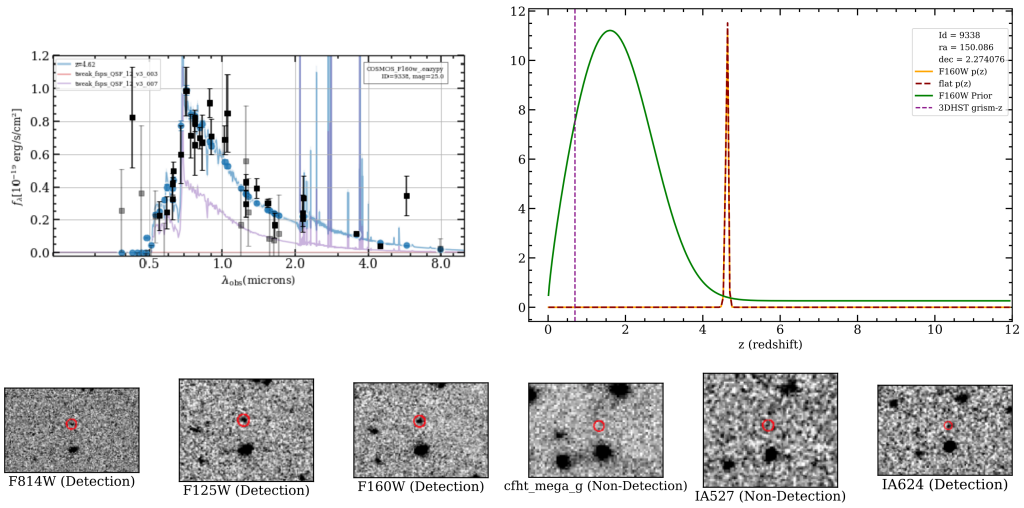

Figure 4.10: Object 9338 from COSMOS, z = 4.62.

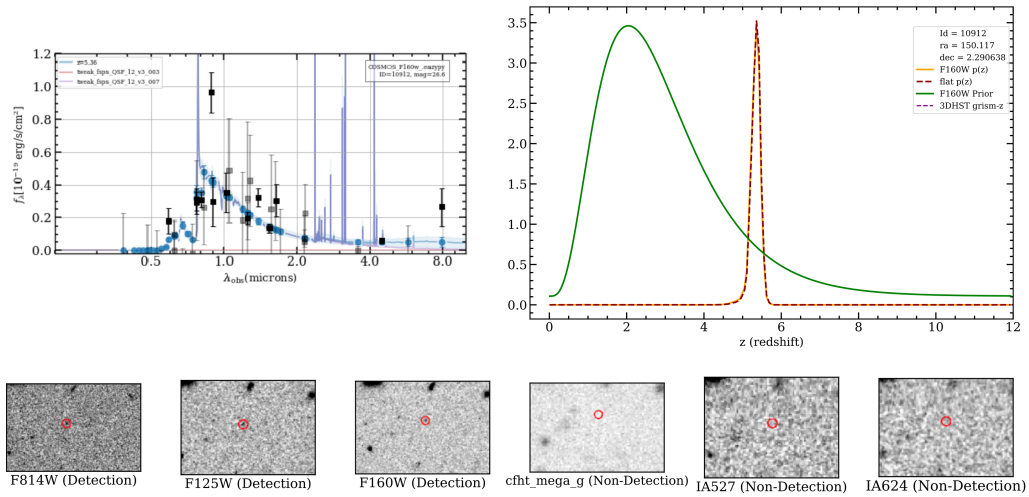

Figure 4.11: Object 10912 from COSMOS, z = 5.36.

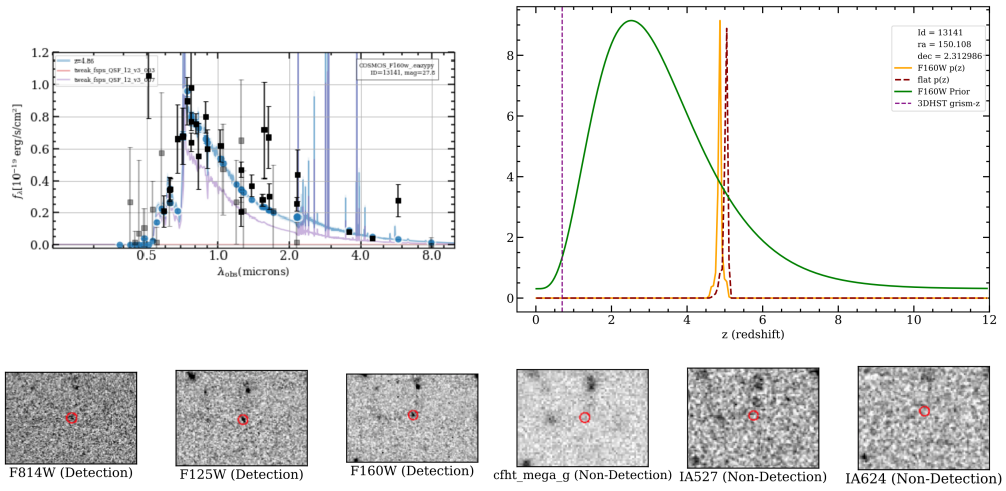

Figure 4.12: Object 13141 from COSMOS, z = 4.86.

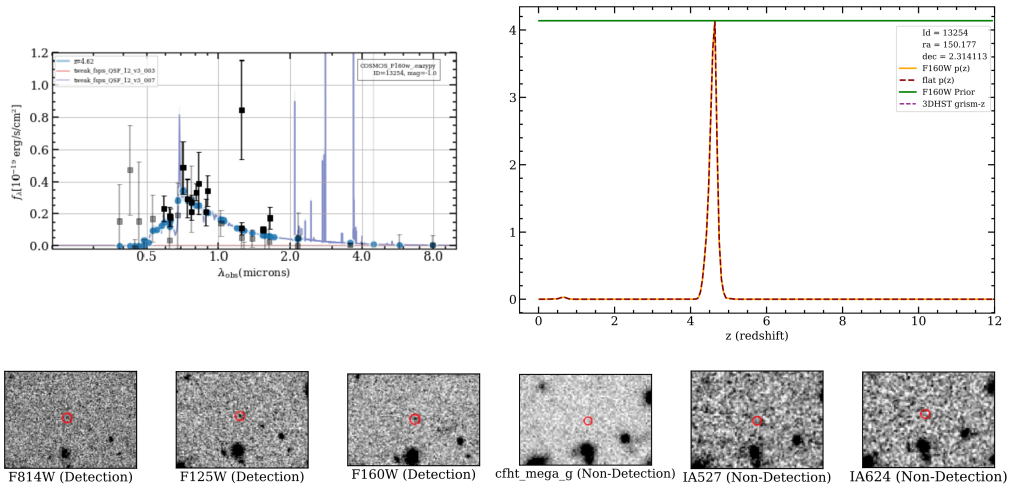

Figure 4.13: Object 13254 from COSMOS, z = 4.62.

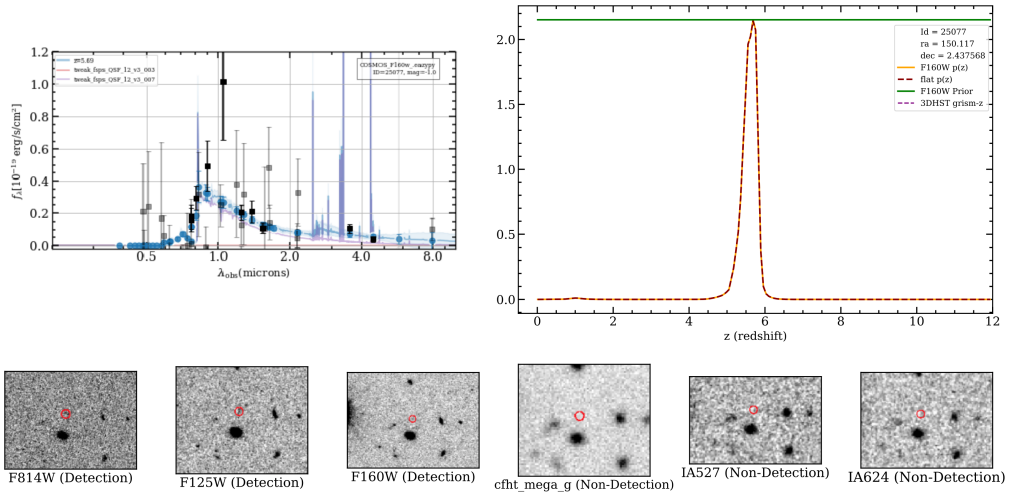

Figure 4.14: Object 25077 from COSMOS, z = 5.69.

4.3 GOODSN Data

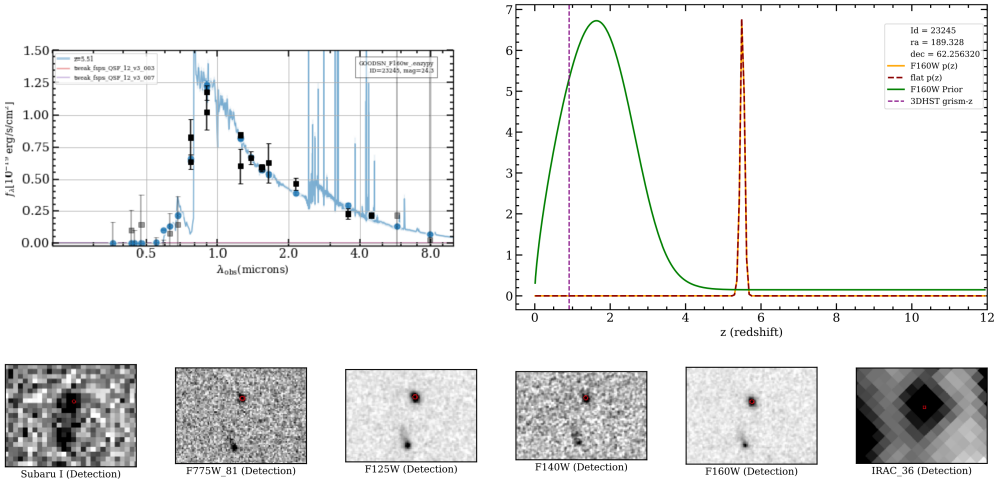

Figure 4.15: Object 23245 from GOODSN, z = 5.51.

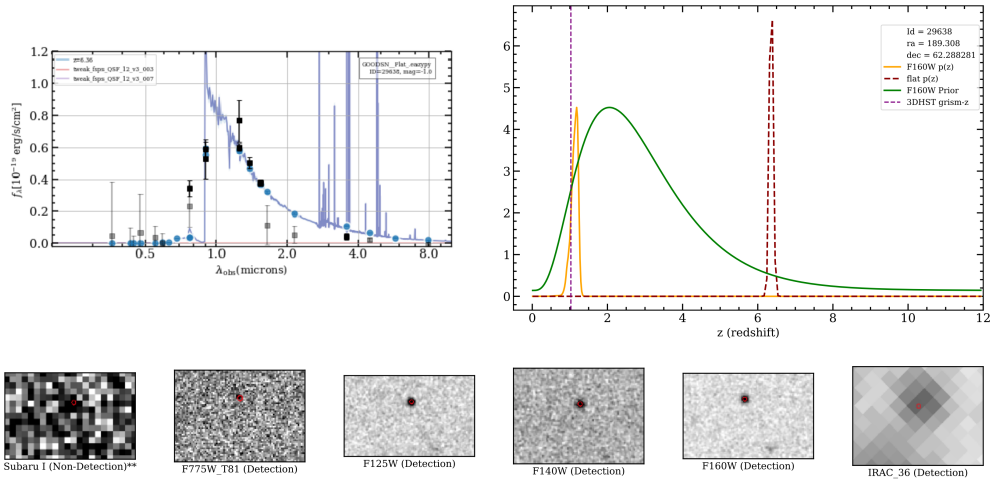

Figure 4.16: Object 29638 from GOODSN, z = 6.36.

4.4 GOODSS Data

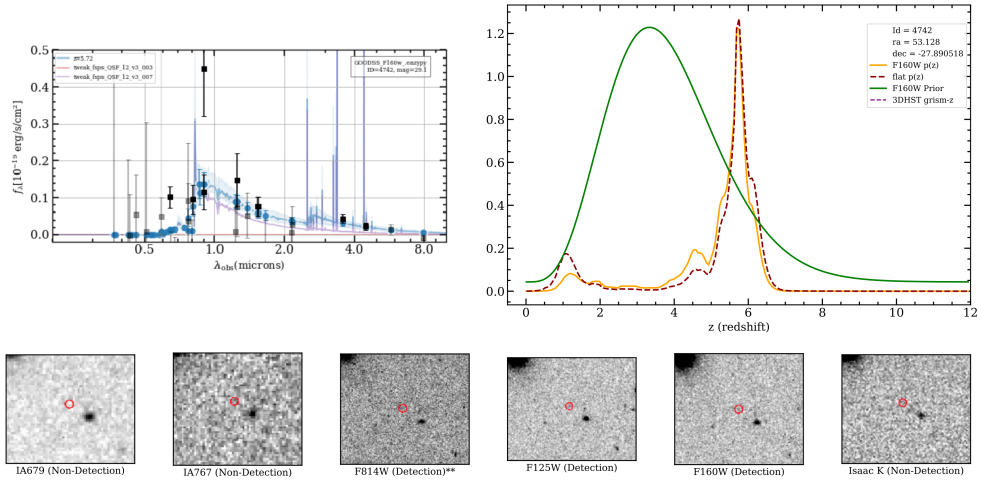

Figure 4.17: Object 4742 from GOODSS, z = 5.72.

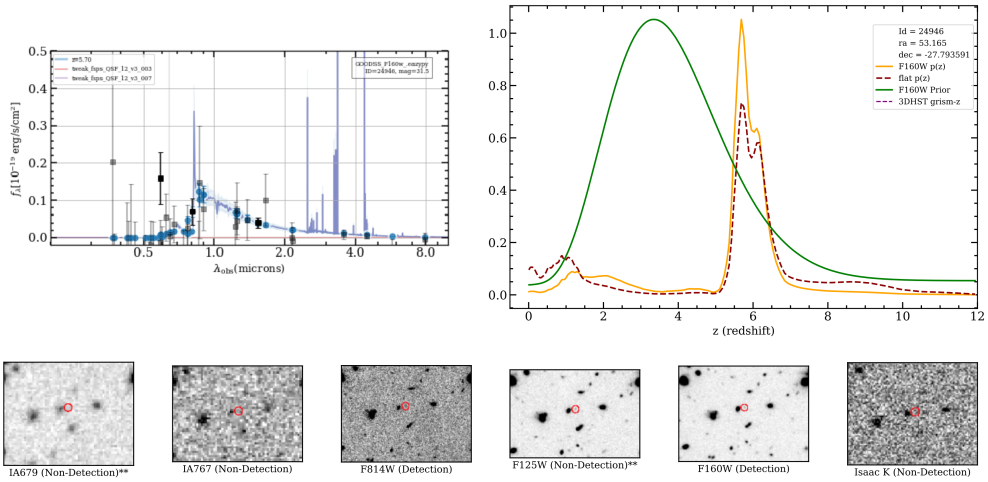

Figure 4.18: Object 24946 from GOODSS, z = 5.70.

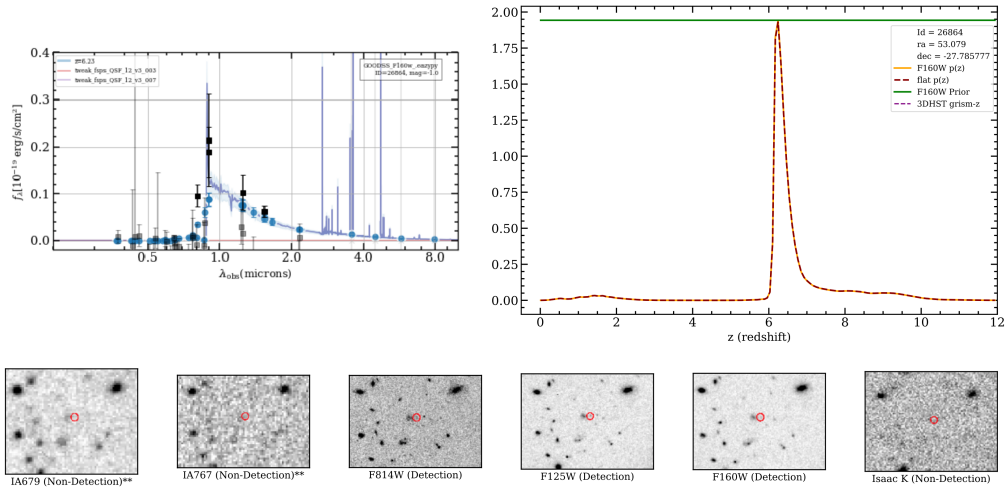

Figure 4.19: Object 26864 from GOODSS, z = 6.23. False Positive.

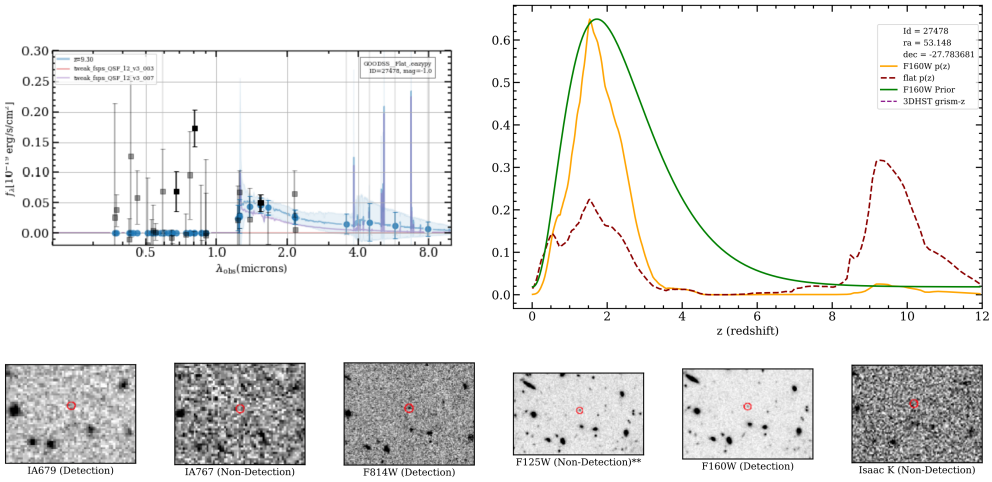

Figure 4.20: Object 27478 from GOODSS, z = 9.30. False Positive.

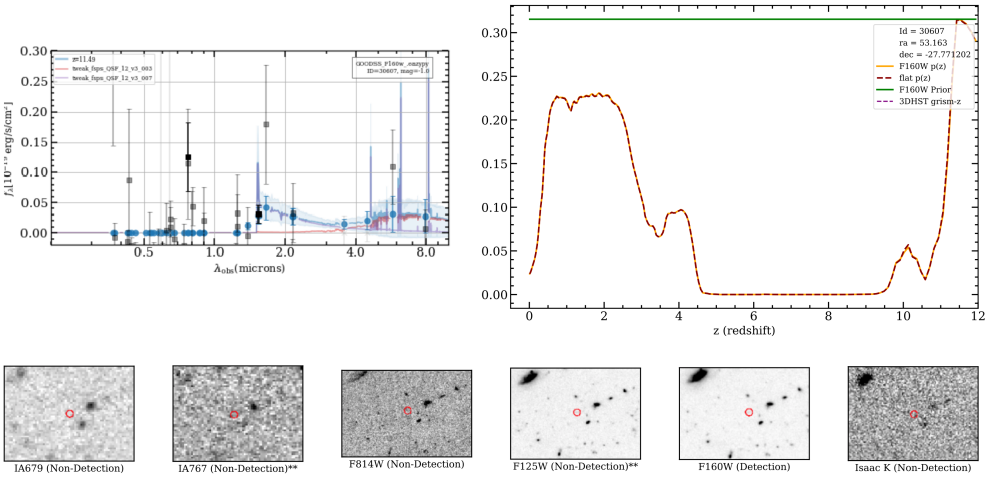

Figure 4.21: Object 30607 from GOODSS, z = 11.49.

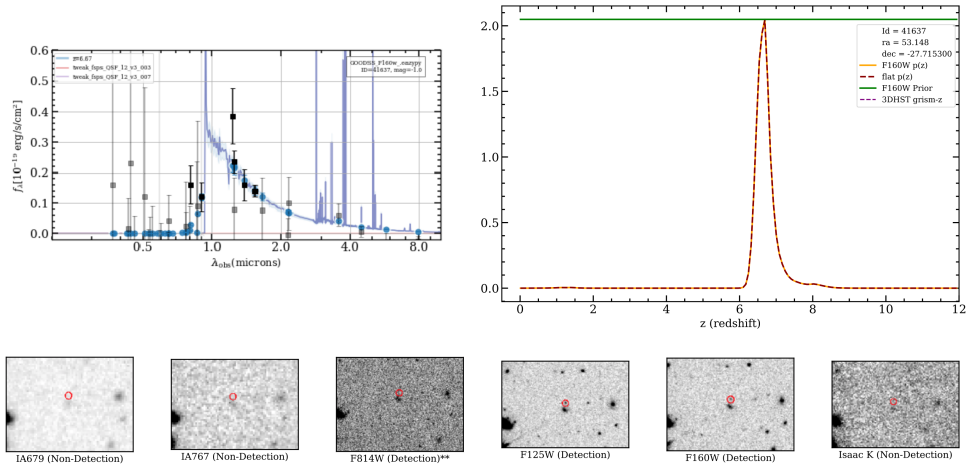

Figure 4.22: Object 41637 from GOODSS, z = 6.66.

4.5 UDS Data

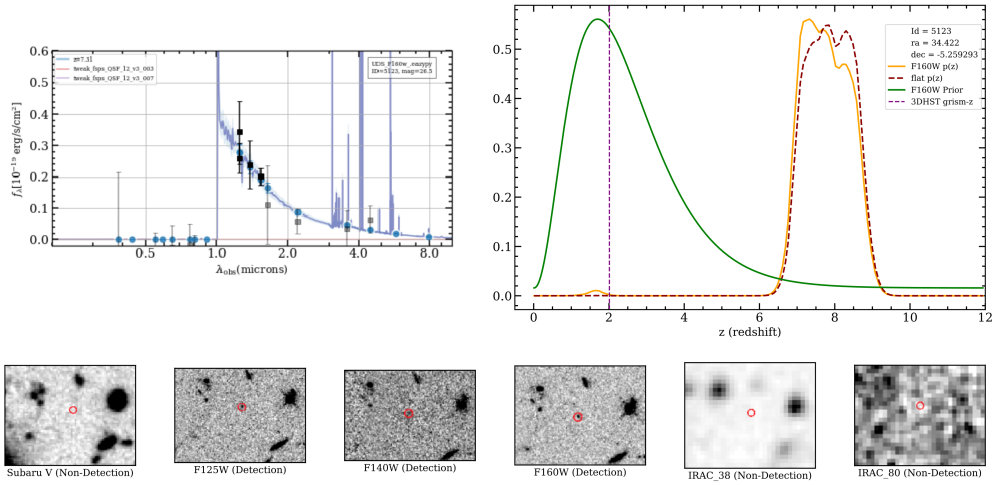

Figure 4.23: Object 5123 from UDS, z = 7.31.

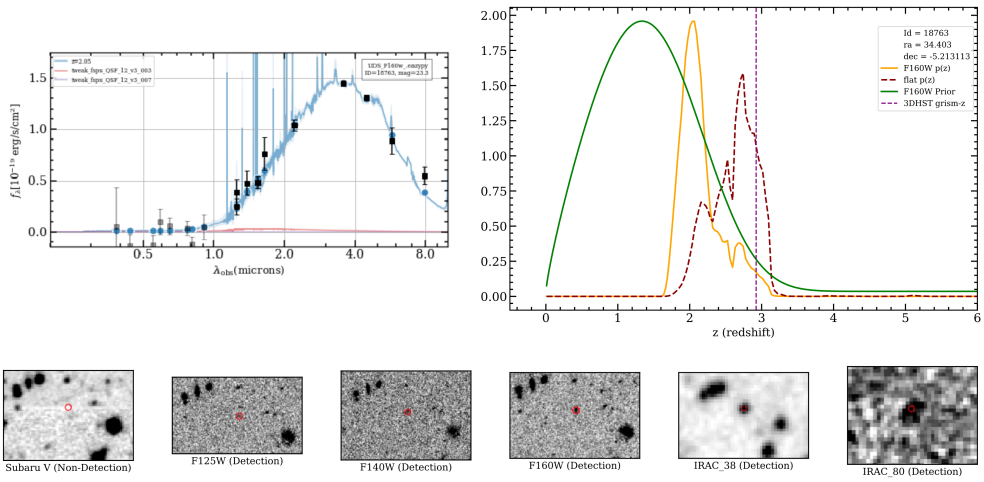

Figure 4.24: Object 18763 from UDS, z = 2.05. False Positive.

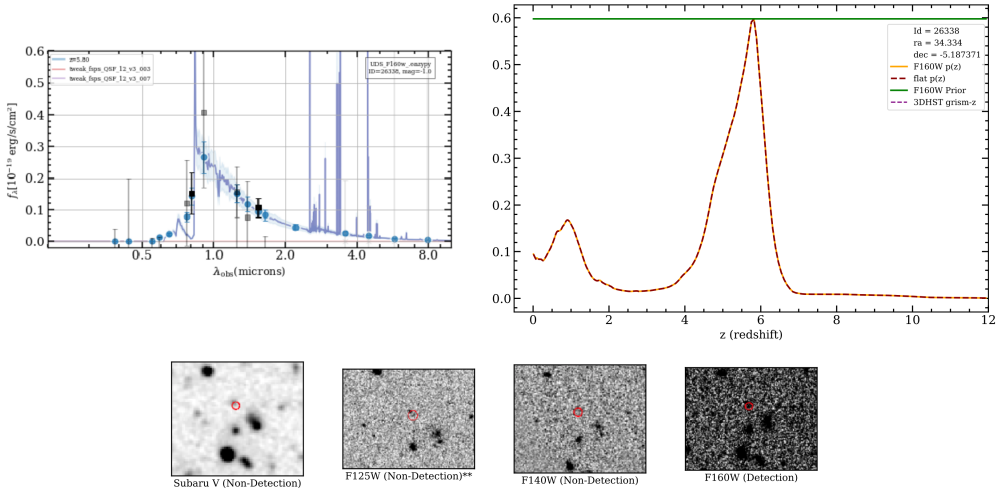

Figure 4.25: Object 26338 from UDS, z = 5.80

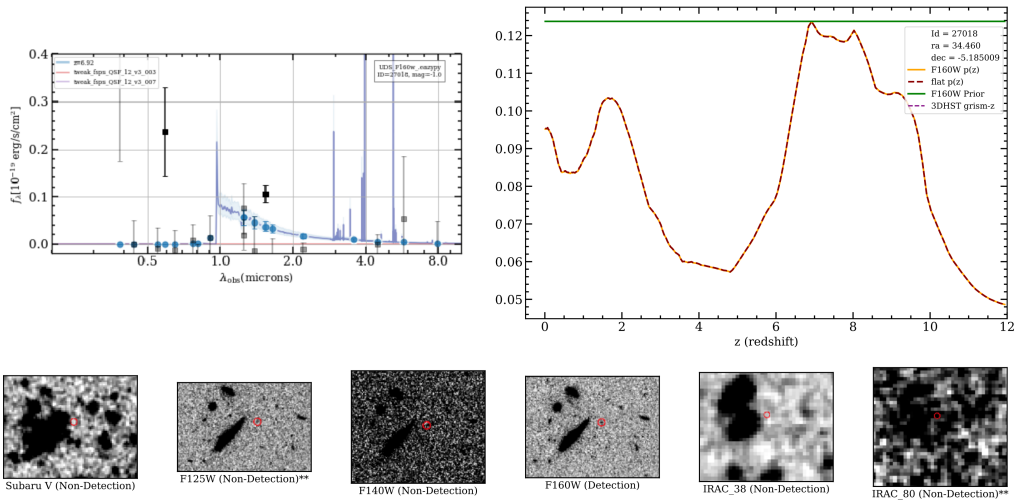

Figure 4.26: Object 27018 from UDS, z = 6.92

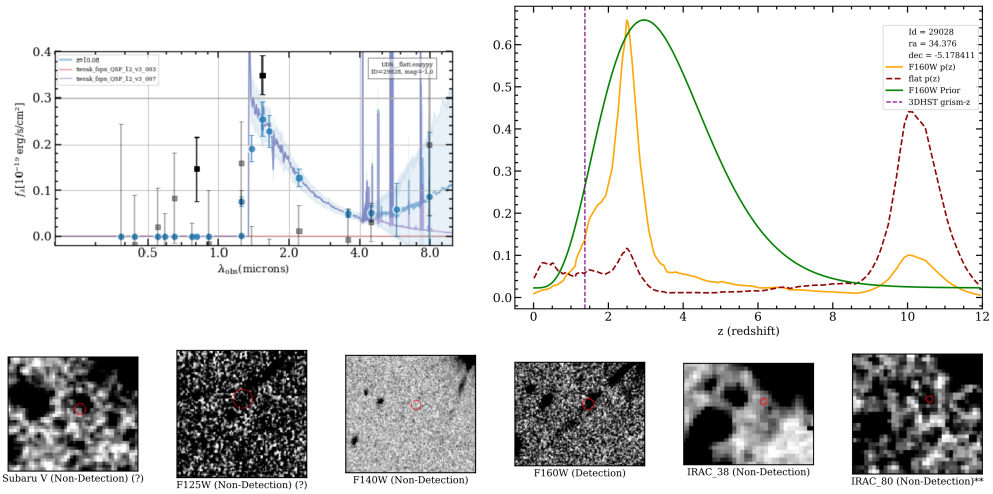

Figure 4.27: Object 29028 from UDS, z = 10.08. False Positive

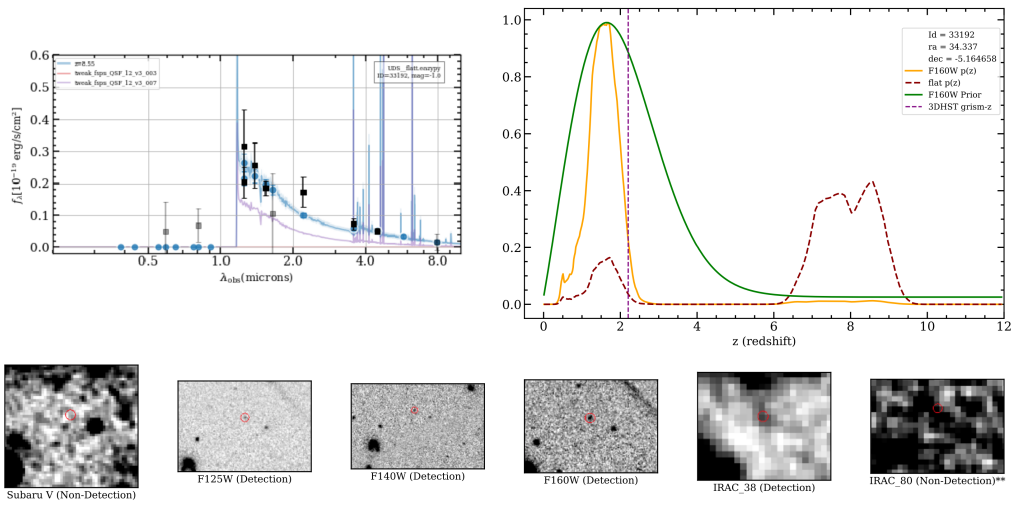

Figure 4.28: Object 33192 from UDS, z = 8.55

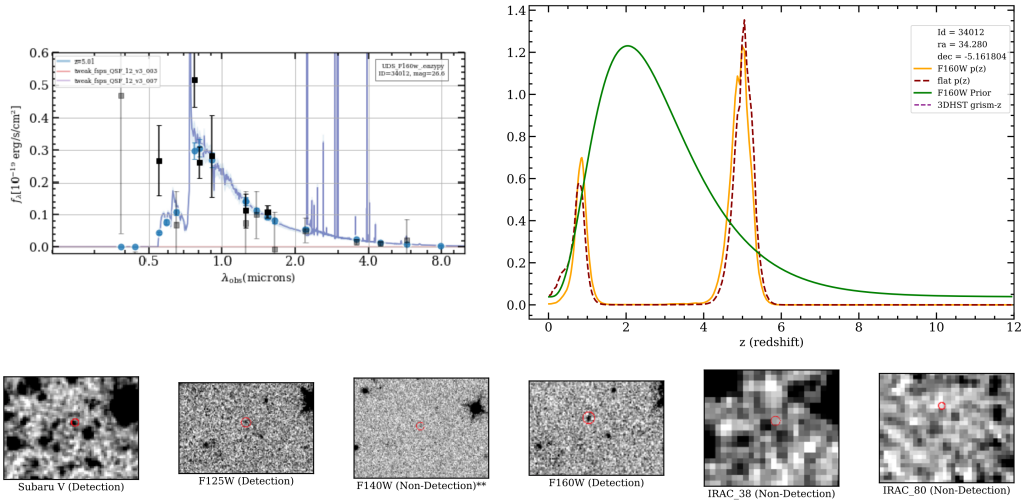

Figure 4.29: Object 34012 from UDS, z = 5.01

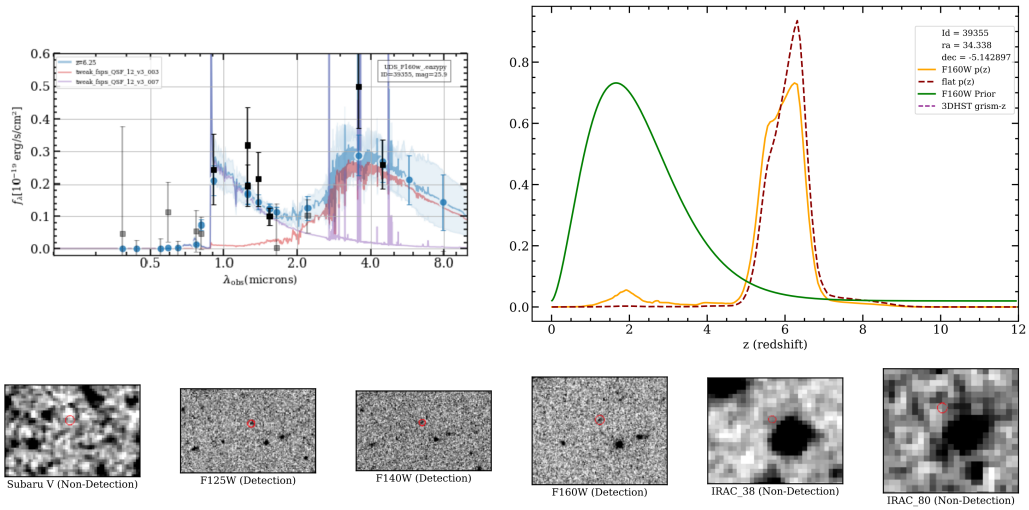

Figure 4.30: Object 39355 from UDS, z = 6.25

APPENDIX B: Iterative Analysis Data

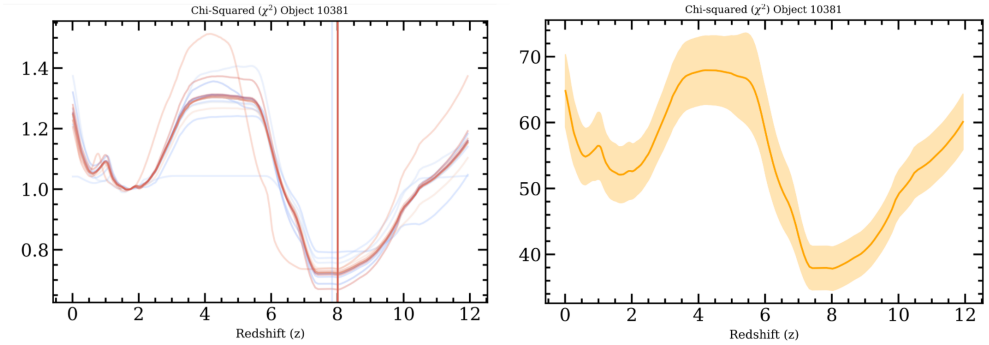

Figure 4.31: (Left) χ^2 Distribution for iterative testing for Object 10381 from the AEGIS field. (Right) The average χ^2 with the standard deviation for object 10381.

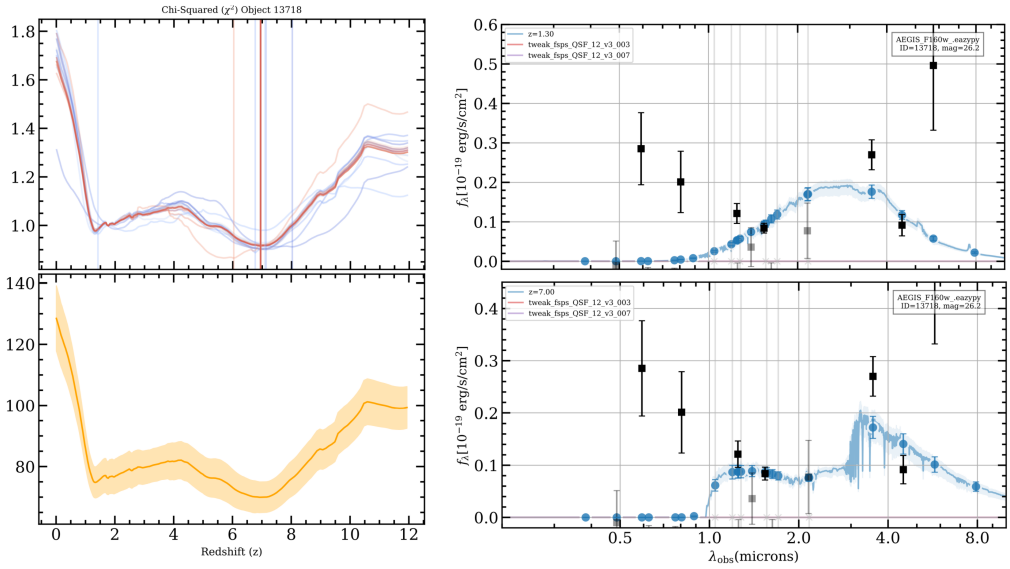

Figure 4.32: (Top Left) χ^2 Distribution for iterative testing for Object 13718 from the AEGIS field. (Bottom Left) The average χ^2 with the standard deviation for object 13718. (Top Right) Original SED, (Bottom Right) Second option SED for new redshift. The new SED did not show much improvement, and thus was labeled as a false positive.

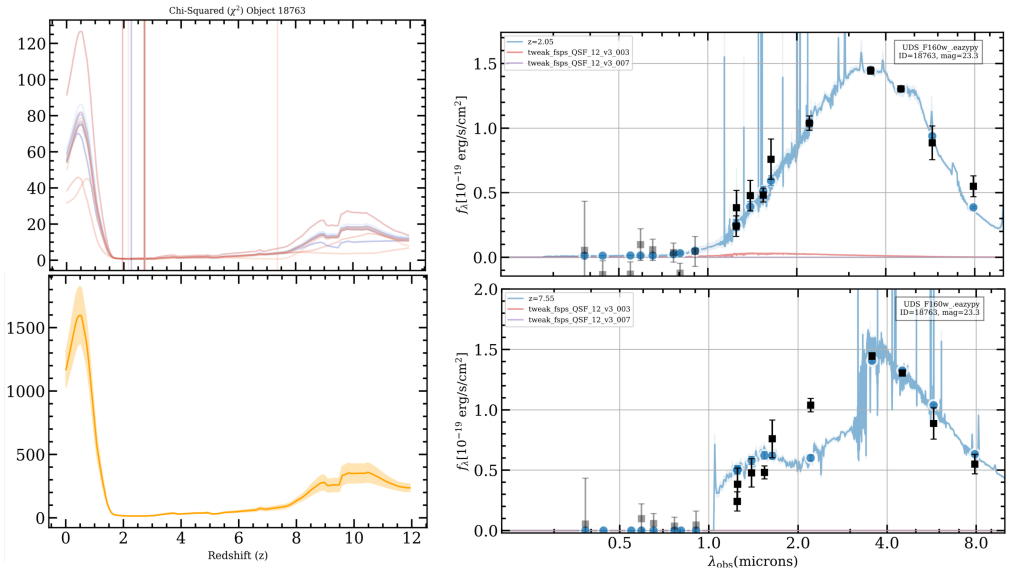

Figure 4.33: (Top Left) χ^2 Distribution for iterative testing for Object 18763 from the UDS field. (Bottom Left) The average χ^2 with the standard deviation for object 18763. (Top Right) Original SED, (Bottom Right) Second option SED for new redshift. The new SED did not show much improvement, and thus was labeled as a false positive.

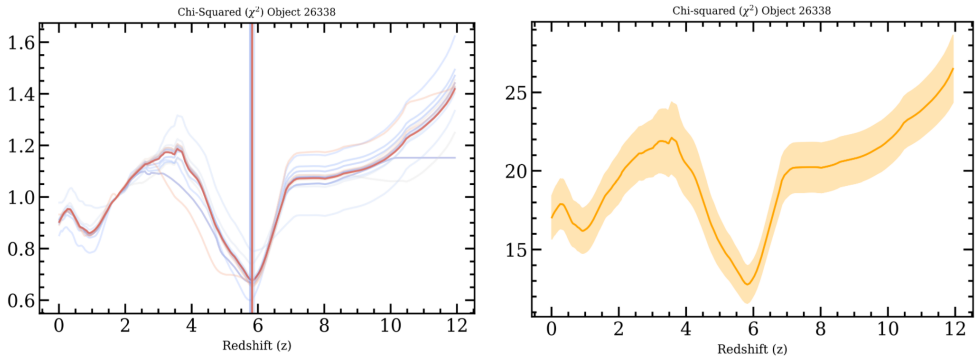

Figure 4.34: (Left) χ^2 Distribution for iterative testing for Object 26338 from the UDS field. (Right) The average χ^2 with the standard deviation for object 26338.

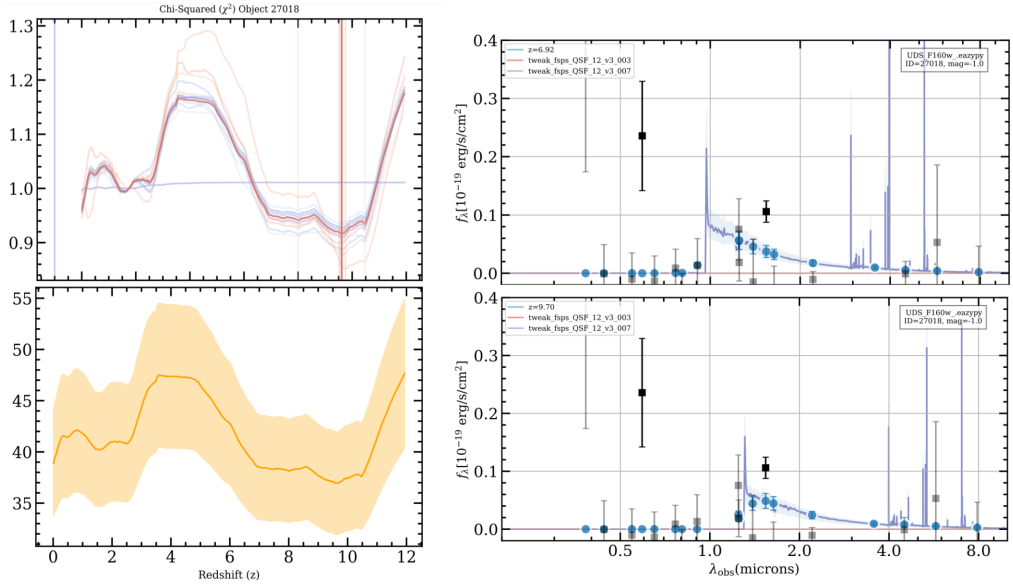

Figure 4.35: (Top Left) χ^2 Distribution for iterative testing for Object 27018 from the UDS field. (Bottom Left) The average χ^2 with the standard deviation for object 27018. (Top Right) Original SED, (Bottom Right) Second option SED for new redshift.

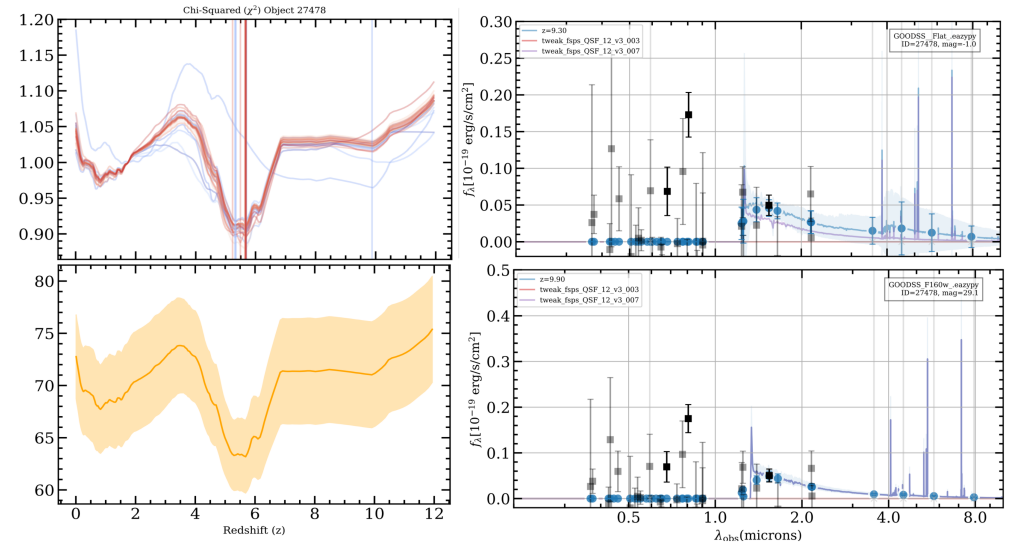

Figure 4.36: (Top Left) χ^2 Distribution for iterative testing for Object 27478 from the GOODSS field. (Bottom Left) The average χ^2 with the standard deviation for object 27478. (Top Right) Original SED, (Bottom Right) Second option SED for new redshift. The new SED did not show much improvement, and thus was labeled as a false positive.

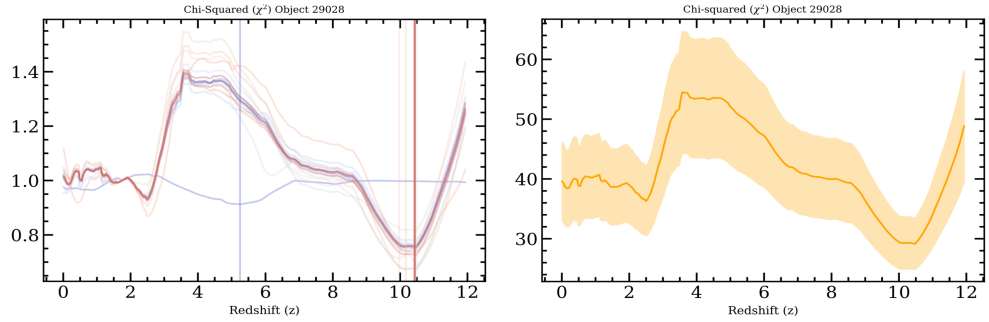

Figure 4.37: (Top Left) χ^2 Distribution for iterative testing for Object 29028 from the UDS field. (Bottom Left) The average χ^2 with the standard deviation for object 29028. (Top Right) Original SED, (Bottom Right) Second option SED for new redshift. The new SED did not show much improvement, and thus was labeled as a false positive.

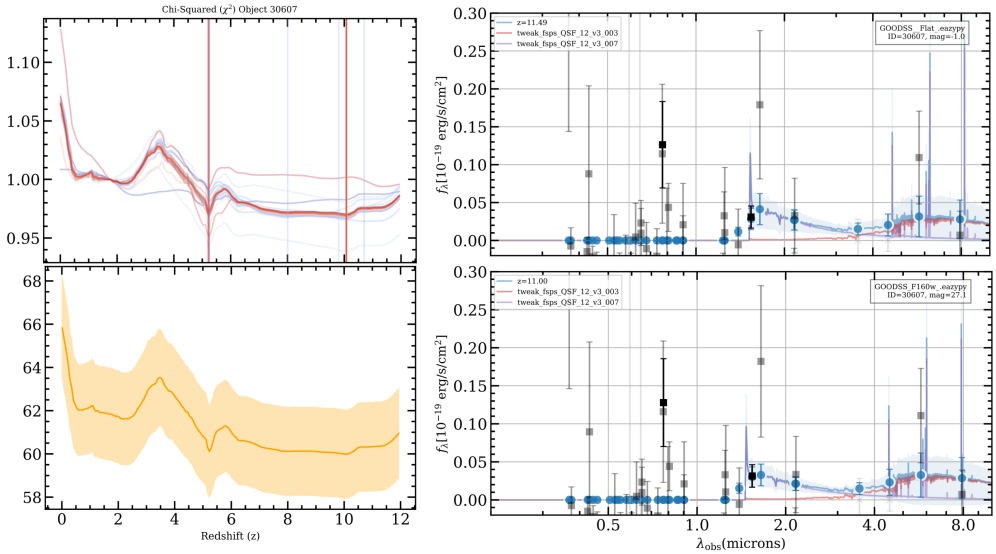

Figure 4.38: (Top Left) χ^2 Distribution for iterative testing for Object 20607 from the GOODSS field. (Bottom Left) The average χ^2 with the standard deviation for object 30607. (Top Right) Original SED, (Bottom Right) Second option SED for new redshift. The new SED did not show much improvement, and thus was labeled as a false positive.